Propagation of radiative shock waves in an inhomogeneous cosmic medium

1972 J. Phys. A: Gen. Phys. 5 1409

(http://iopscience.iop.org/0022-3689/5/9/014)

J. Phys. A: Gen. Phys., Vol. 5, September 1972. Printed in Great Britain.

Propagation of radiative shock waves in an inhomogeneous cosmic medium

T L CHOW

California State College, Stanislaus, Turlock, California 95380, USA

MS received 23 February 1972

Abstract. The propagation of two strong radiative shocks moving opposite in an inhomogeneous cosmic medium is calculated by using a 'modified' characteristic method. It is found that the shock propagation is seriously affected by radiation losses and by the inhomogeneity of the medium; the cooled and recombined post-shock gas first appears near the shock front. This differs from results derived from steady state solutions, which predict that the condensation should appear first at the contact surface.

1. Introduction

During a search for a possible origin of the high velocity neutral hydrogen gases at high galactic latitudes, we calculated the consequences when high momentum extragalactic clouds collide with galactic gases; the extragalactic gases having initial velocities of about 500 km s^{-1} with respect to the local standard of rest (Oort 1966). After collision, two strong radiative shocks appear and move away from the contact surface into the galactic and extragalactic gases respectively. Both gases are ionized during this interaction, and they will recombine after radiating their surplus energies.

In examining the shock propagation, the change in the flow pattern behind the shock fronts caused by the cooling, the reflected compression waves from the fronts, etc, should be included in the treatment. So we have to solve the hydrodynamic equations. Limited to a one dimensional plane flow of a nonviscous and nonthermal conducting ideal gas, the solutions of the hydrodynamic equations on a modified characteristic grid were obtained. At shock fronts, these solutions are subject to the Rankine–Hugoniot relations. We take into account both the density variation of the galactic gas and radiation losses. We found that the shock propagation is seriously affected by radiation losses and by the inhomogeneity of the medium, and condensation (cooled and recombined gas) first appears near the galactic shock front. This differs from results derived from steady state solutions, which predict that the condensation should appear first at the contact surface. This we shall discuss after we present our results.

2. Basic equations

We use the method of Lagrange undetermined multipliers (Courant and Friedricks 1948).

The equations of motion in standard form are

$$\text{Equation of continuity} \qquad \frac{\mathrm{D}\rho}{\mathrm{D}t}+\rho\frac{\partial u}{\partial x}=0 \tag{1}$$

$$\text{Equation of motion} \qquad \rho\frac{\mathrm{D}u}{\mathrm{D}t}+\frac{\partial P}{\partial x}=0 \tag{2}$$

$$\text{Equation of conservation of energy} \qquad \rho\frac{\mathrm{D}\epsilon}{\mathrm{D}t}-\frac{P}{\rho}\frac{\mathrm{D}\rho}{\mathrm{D}t}=-Q \tag{3}$$

where P, ρ, u are the gas pressure, gas density and the fluid velocity respectively, $\epsilon=\{1/(\gamma-1)\}(P/\rho)+\frac{1}{2}V_{\mathrm{i}}^2,\frac{1}{2}V_{\mathrm{i}}^2$ is the ionization energy per gramme and Q is the energy loss per unit volume per second. We now transform the standard form into characteristic form as follows:

$$\mathrm{d}p+\gamma\frac{p}{c}\,\mathrm{d}u+(\gamma-1)Q\,\mathrm{d}t=0 \tag{4a}$$

along

$$\mathrm{d}x=(u+c)\,\mathrm{d}t. \tag{4b}$$

$$\mathrm{d}p-\gamma\frac{p}{c}\,\mathrm{d}u+(\gamma-1)Q\,\mathrm{d}t=0 \tag{5a}$$

along

$$\mathrm{d}x=(u-c)\,\mathrm{d}t. \tag{5b}$$

$$(1-\gamma)\,\mathrm{d}p+\frac{2\gamma p}{c}\,\mathrm{d}c+(\gamma-1)Q\,\mathrm{d}t=0 \tag{6a}$$

along

$$\mathrm{d}x=u\,\mathrm{d}t. \tag{6b}$$

In all calculations, the characteristic equations are placed in finite difference form by replacing the differential coefficient by a difference ratio over the interval and replacing other quantities by the arithmetic mean over the interval. This ensures that errors due to the finite size of mesh are of the order of the square of the mesh size. Furthermore, we define the mesh points in advance in both space and time and perform the interpolations as the calculations proceed. This has the advantage that interpolations required are always one dimensional (Hoskin 1965).

At the shock front, we have the Rankine–Hugoniot relations (Savedoff *et al* 1967)

$$\frac{\rho}{\rho'}=\frac{\gamma-\{1+(\gamma^2-1)(V_{\mathrm{i}}/V_{\mathrm{s}})^2\}^{1/2}}{\gamma+1} \tag{7}$$

$$p'=\rho V_{\mathrm{s}}^2(1-\rho/\rho') \tag{8}$$

$$u'=V_{\mathrm{s}}(1-\rho/\rho') \tag{9}$$

where V_{s} is the shock velocity, and all primed quantities refer to the post-shock gases. These, together with an equation of state, give four equations to solve for five unknowns, u', T', V_{s}, p', and ρ', assuming that conditions are known in front of the shock front. Thus, if one variable is assumed, we can solve for the other unknowns.

3. Physical conditions

The calculations were performed for an initial density ratio ρ_1/ρ_2 of unity at $t = 0$ (ie with equal densities in the galactic and extragalactic gases at collision) under the following physical conditions or restrictions:

(i) The extragalactic cloud is taken to be homogeneous, and the galactic gas density n_H is represented by

$$n_H = n_0 \exp(-z/q_0) \qquad \text{H atoms cm}^{-3}$$

where z is measured in parseconds above the plane, and the scale height $q_0 = 120$ pc, $n_0 = 0{\cdot}7$ H atoms cm^{-3}. This layer ends at about $z = 600$ pc, beyond which lies the corona. The shocks are assumed to begin at this height.

(ii) The radiation loss rates are taken from Pottasch (1965), with H, He, O, C, Mg, Si, and Ne abundances of 1, 10^{-1}, 10^{-3}, $10^{-3{\cdot}3}$, 10^{-4}, 10^{-4}, 10^{-4} respectively and ionization equilibria according to House (1964). Although hydrogen and helium dominate in abundances, the energy losses are mainly caused by collisional transitions in the heavier ions.

(iii) Both the pre-shock and the post-shock gases are taken to be perfect gases

$$P = \frac{k\rho}{\mu H}T \qquad P' = \frac{k\rho'}{\mu' H}T'.$$

The notations are the usual, μ and μ' denote mean particle mass expressed in units of the mass of the proton. The post-shock gas is a rarefied plasma, in which the density is still low and the mean free path of the particles is very large, so that the mean energy of the Coulomb interactions between neighbouring particles is small in comparison with the mean thermal energy of the particles and we can neglect it; thus the post-shock gas can be considered as a perfect gas.

(iv) The precursor effects upon the pre-shock state are neglected, and the following uniform conditions ahead of the shock front are adopted: the density, pressure and temperature take unperturbed values, and in particular, both gases are taken to be originally at a temperature of about 100 K.

(v) Values of the ionization parameters are taken from Savedoff *et al* (1967)

$$\mu_1 = \mu_2 = 1{\cdot}273 \qquad \mu_1' = \mu_2' = 0{\cdot}625$$
$$\mu_e = 1{\cdot}2 \qquad V_i = 50 \text{ km s}^{-1}.$$

where $\frac{1}{2}V_i^2$ represents the ionization energy per gramme. Values of some initial parameters connected with the two shocks created by a gas collision at relative velocity of 500 km s^{-1} are also taken from Savedoff *et al* (1967)

$$\rho_1/\rho_1' = 0{\cdot}242 \qquad S_1 = 330 \text{ km s}^{-1} \qquad S_2 = 170 \text{ km s}^{-1}$$
$$T_1' = T_2' = 1{\cdot}52 \times 10^6 \text{ K}$$

where S_1 and S_2 are the galactic shock velocity and the cloud shock velocity relative to the galactic gas, respectively†.

† We work in a coordinate system in which the galactic gas is at rest and the extragalactic gas approaches us with a velocity of about 500 km s^{-1}. We also reserve index (1) for galactic gas and index (2) for extragalactic gas. All primed quantities refer to the post-shock gases.

4. Results

At first, the spatial temperature profile increases smoothly from the galactic shock front to the cloud shock front, the negative temperature gradient becoming more negative with increasing time. The pressure and density profiles decrease smoothly from the galactic shock front to the cloud shock front, although the absolute density and pressure increase slightly with increasing time. This temporal increase gradually slows until after about 7×10^5 yr (at this age, $T_1' = 5{\cdot}8 \times 10^5$ K), when there also appears on the galactic side a 'depression' in the initial smooth temperature and pressure profiles as shown in figures 1 to 3. Subsequently, this 'depression' acquires the form of a 'deep well' as shown in figure 4. Figure 5 shows the development of the pressure dip.

This result differs from those derived from steady state solutions, which predict that these dips should appear first at the contact surface. These previous treatments neglect the change in the flow pattern caused by the cooling contraction of the post-shock gas. The cooling causes the shocks to slow down with respect to the gas they are penetrating, and this gives rise to complications behind the shock fronts describable as compression and expansion waves. For shocks in colliding nonhomogeneous gas clouds, the complications behind the shock fronts are far greater, because of both the cooling contraction of the post-shock gas and the effects of external density and pressure variations upon the shock propagation. This we now discuss.

5. Discussion

When the galactic shock is propagated towards the galactic plane, its strength, defined either by the pressure ratio across the front $Y_1 = P_1'/P_1$, or by the shock velocity S_1, is decreased with increasing time. This decrease produces a continuous system of compression waves, which slow the motion of the contact surface towards the galactic

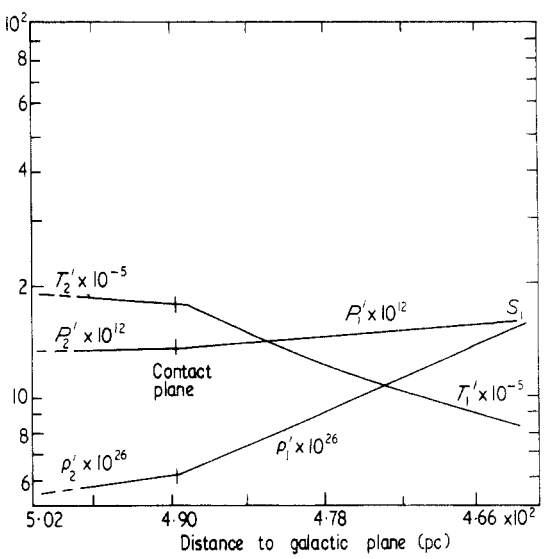

Figure 1. Spatial temperature, pressure and density profiles for the gases behind shocks at $t = 4{\cdot}863 \times 10^5$ yr, $S_1 = 0{\cdot}242 \times 10^8$ cm s^{-1} and $S_2 = 0{\cdot}126 \times 10^8$ cm s^{-1}.

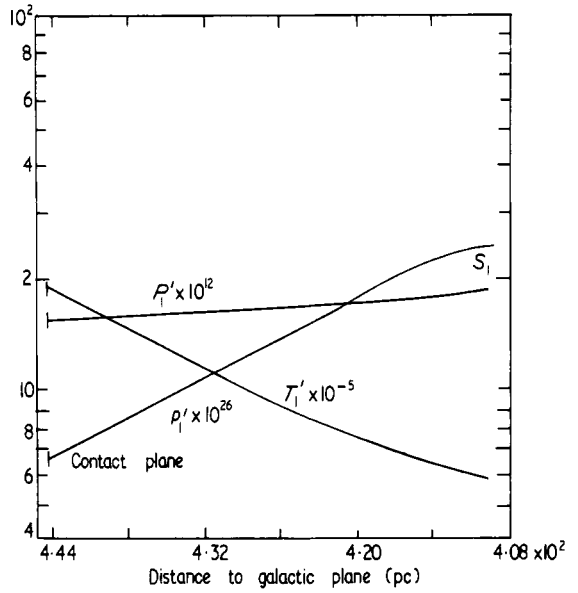

Figure 2. Spatial temperature, pressure, and density profiles for the gases behind the galactic shock at $t = 7{\cdot}14 \times 10^5$ yr, $S_1 = 0{\cdot}208 \times 10^8$ cm s^{-1}. Temperature inversion begins to develop.

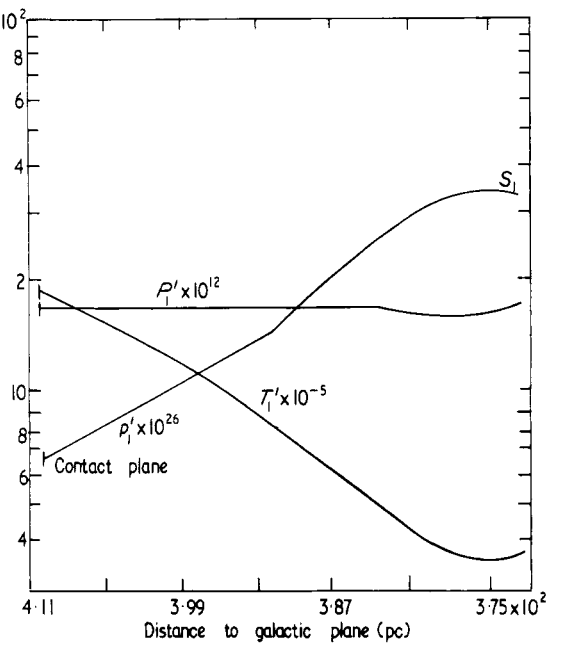

Figure 3. Spatial temperature, pressure, and density profiles for the gases behind the galactic shock at $t = 9{\cdot}041 \times 10^5$ yr, $S_1 = 0{\cdot}1715 \times 10^8$ cm s^{-1}.

plane. The deceleration of the contact surface in turn reacts on the galactic shock by generating expansion waves which reduce the galactic shock velocity. The deceleration of the contact surface also gives rise to compression waves which overtake the cloud

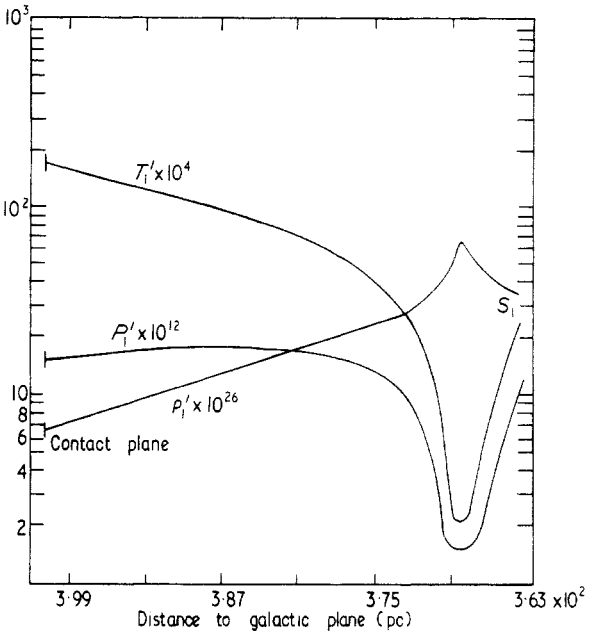

Figure 4. Spatial temperature, pressure and density profiles for the gases behind the galactic shock at $t = 9{\cdot}615 \times 10^5$ yr, $S_1 = 0{\cdot}139 \times 10^8$ cm s^{-1}. The gas at the dip has cooled to 20 000 K.

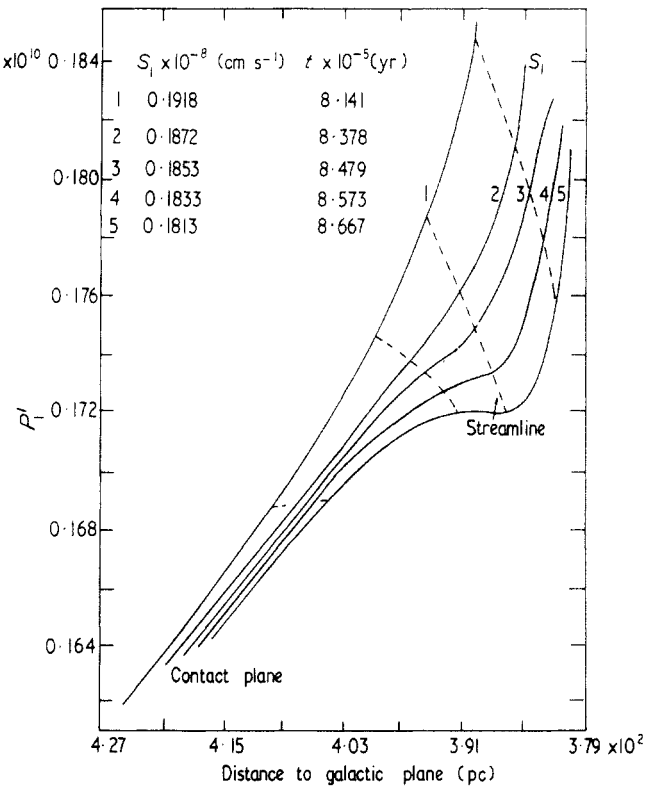

Figure 5. Development of the pressure dip.

shock and increase its strength. The result is smooth spatial pressure and density profiles with the pressure and density decreasing from the galactic shock front to the cloud shock front. The temperature profile is also a smooth curve with temperature increasing from the galactic shock front to the cloud shock front, because of the increasing of the cloud shock strength and the decreasing of the galactic shock strength with increasing time.

Radiation losses and the density and pressure increase of the ambient gas end the smooth behaviour of the pressure, density, and temperature profiles after the shock has moved about one scale height.

5.1. Scale height effects

The increase of $P_1'(=Y_1P_1)$ in time results from the very slow decrease of Y_1 and S_1 with time and from the exponential increase of the ambient pressure P_1. Before the radiation loss becomes important, the shock propagation is only affected by the effects of the external density and pressure variations and both Y_1 and S_1 are expected to decrease very slowly (Savedoff *et al* 1967); for instance, initially the shock propagates at $330\,\mathrm{km\,s^{-1}}$ covering a scale height in $t_{sh} \simeq 3{\cdot}5 \times 10^5$ yr, and at $1{\cdot}52 \times 10^6$ K, $n_e \simeq 0{\cdot}023$, the energy per electron ($\sim 3kT$) is radiated at a rate $5{\cdot}5 \times 10^{-23} n_e\,\mathrm{erg\,s^{-1}}$, hence $t_r \simeq 2 \times 10^7$ yr, thus radiation effects are negligible at this stage compared to scale height effects.

5.2. Radiative effects

As the temperature of the galactic shock wave falls (with concomitant decrease in shock strength), the density and temperature changes increase the radiation loss rates so that this loss becomes important. Thus, the increase of P_1' in time is gradually slowed. When the shock ages to $7{\cdot}89 \times 10^5$ yr, P_1' begins to decrease with increasing time. At this age, $T_1' = 5{\cdot}147 \times 10^5$ K, $Q \simeq 0{\cdot}267 \times 10^{-23}\,\mathrm{erg\,cm^{-3}\,s^{-1}}$, $S_1 \simeq 196\,\mathrm{km\,s^{-1}}$, and $n_e \simeq 0{\cdot}136\,\mathrm{cm^{-3}}$. Using the same argument as before, we find $t_{sh} \simeq 5{\cdot}996 \times 10^5$ yr, and $t_r \simeq 4{\cdot}3 \times 10^5$ yr. Thus, both the radiation loss and the ambient pressure and density variations modify the shock propagation strongly. Figure 5 shows the evolution of P_1' in time for this later stage. Time increases from the left to the right as indicated in the figure. Flow lines are also drawn to indicate how the pressure changes in time. Gas close to the contact surface is still very hot, hence the radiation losses are not strongly felt, thus the pressure close to the contact surface still increases slightly with increasing time in contrast with the dip region, which will be discussed below. After 8×10^5 yr from the beginning, $t_{sh} \simeq 6 \times 10^5$ yr and $t_r \simeq 4 \times 10^5$ yr, hence radiation effects become dominant; the major factors which now determine the features of pressure, temperature, and density profiles are the temperature dependence of the radiation losses and the previous history of the phenomena. In general, if the energy loss increases as the temperature decreases, there is no stable value of the temperature, and the system is unstable (Field 1962). This may be seen from the following qualitative argument: the effect of radiation losses is to reduce the pressure and to increase the density along a flow line as the temperature falls. The density increase and the temperature drop both increase the radiation loss rates; this increase in turn causes a further pressure drop and a further density increase until the reduced pressure can no longer remain sufficient to balance the momentum flux of the incoming gases, hence

the post-shock gas will be compressed and the dips in temperature and pressure profiles are gradually formed.

A quantitative condition for this growth follows on considering perturbations of the flow. We consider a small perturbation $\delta u'$, $\delta p'$, $\delta\rho'$, etc on a desired solution $u'(x,t)$ etc, and investigate whether the perturbation grows with increasing time (Von Neumann and Richtmyer 1950). To do this, we replace u', p', etc, by $u'+\delta u'$, $p'+\delta p'$, etc in equations (1) to (3), and get a set of three simultaneous linear differential equations for $\delta u'$, $\delta p'$, etc. Their coefficients depend on the desired solutions u, p, etc. We treat these coefficients as constants in a small region and look for solutions of the form $\delta u' = \delta u_0 \exp(\delta t + ikx)$, etc, where u_0, etc, and k, α are constants and k is real. Substitution of these into the simultaneous linear differential equations for $\delta u'$, $\delta p'$, etc, leads to three simultaneous homogeneous linear equations in δu_0, δp_0, etc. The vanishing of the determinant of these equations yields an equation connecting k and α. By solving this equation for α with a given k, we can determine whether a given Fourier component of the perturbation $\delta u' = \delta u_0 \exp(\alpha t + ikx)$ etc, grows with increasing time. The real part of the sum of the three roots of α is independent of k and satisfies

$$\mathrm{Re}(\Sigma\alpha) \geqslant \frac{1}{\rho'}\left\{\frac{\gamma+2}{3}\frac{\mathrm{d}\rho'}{\mathrm{d}t} - \frac{\gamma-1}{3R}\left(\frac{\partial Q}{\partial T'}\right)_{\rho'}\right\}.$$

It is seen that if $\mathrm{Re}(\Sigma\alpha) > 0$, then there exists at least one root with $\alpha > 0$. For high temperatures $(\partial Q/\partial T')_{\rho'} < 0$, hence during compression the system is unstable, and the growth of the dips is formed both by the compression and the energy loss term for $T' > 3\times 10^5$ K. For lower temperatures $(\partial Q/\partial T')_{\rho'} > 0$, hence $\mathrm{Re}(\Sigma\alpha)$ may be negative, we cannot find any useful upper limit on α because of algebraic complexity. In our calculations which end at 2×10^4 K, it takes only three steps (of 5000 yr per step) to evolve from 2×10^5 K to 2×10^4 K. It is desirable to repeat this part of the calculations with small time intervals to determine more precisely the evolution of the dips when radiation losses decrease with decreasing temperature.

5.3. Effects of variation in parameters

Our results depend strongly on the radiative loss rates. For example, in testing the initial program, the radiative loss rate Q/n_e^2 was raised by a factor 10^3; we then got a slightly asymmetric solution with respect to the contact surface, with the pressure behind the galactic shock slightly higher than that behind the cloud shock because of the exponential increase of the ambient pressure P_1. The spatial pressure and temperature decreased smoothly from the two shocks to the contact surface, and the pressure behind the galactic shock decreased with increasing time. This is due to the fact that the radiative effects have been strongly felt already by the shock from the beginning. Thus, the minimum of the dip in the spatial pressure and temperature profiles appears at the contact surface.

Our calculations also depend on n_0, q_0, and z. For instance, a reduction of the value of n_0 will increase $t_r \propto (1/n_0)\exp\{(z-x)/q_0\}$ appreciably, but its effect on t_{sh} is not very marked, we may find some value of n_0 for which t_{sh} is less than t_r and our flow is dominated by scale height effects; thus, the dips in pressure and temperature profiles may not occur at all.

An increase in z will increase the cooling time and the shock displacement, but the qualitative features of our results will probably be unchanged. An increase in z forces

$t_r > t_{sh}$ initially, as the galactic shock propagates toward the plane, t_r decreases following on the density increase and the temperature drop, whereas t_{sh} increases because of the decrease of the shock velocity.

An increase in q_0 increases t_{sh} and the scale height effects decline.

5.4. The precursor effects

The precursor effect upon the pre-shock state was not included in our treatment. Depending on the particular conditions, either photoionization or electron diffusion from the post-shock gas can affect the pre-shock state. The electron diffusion is negligible here. This may be seen from the following argument. The electron diffusion in a region with dimensions of the order of x will create a space charge $e(n_i - n_e)$. This gives rise to an electric potential tending to restore neutrality. But in the absence of external fields, the potential difference is maintained only by the thermal motion of the electrons; consequently, the potential energy eV of the electrons cannot exceed a value of the order of kT, that is $V \sim kT/e$. From Poisson's equation

$$\frac{d^2V}{dx^2} = 4\pi e(n_i - n_e)$$

we have approximately

$$\frac{kT}{ex^2} = 4\pi e(n_i - n_e).$$

Hence

$$\frac{n_i - n_e}{n} = \frac{kT}{4\pi e^2 n x^2} = \left(\frac{h}{x}\right)^2$$

where h, the Debye distance, is given by

$$h = \left(\frac{kT}{4\pi n e^2}\right)^{1/2} = 6{\cdot}9\left(\frac{T}{n}\right)^{1/2}.$$

Thus, over the Debye distance, n_i can deviate appreciably from n_e. But h is less than 10^{-10} pc here, and the charge separation over such a small distance is not of interest to us at all. We wish to know how much charge separation can occur over a distance of the order of the mean free path λ of the electron; that is, can the mobile electrons created immediately behind the shock front leak to an appreciable distance ahead of it? The mean free path of the charged particle is approximately given by

$$\lambda = \frac{(kT)^2}{ne^4 \ln \Lambda}$$

where $\ln \Lambda$ has been tabulated by Spitzer (1962), for the present purpose it can be taken to be constant and equal to 30, then

$$\lambda = 1{\cdot}2 \times 10^4 \frac{T^2}{n} \text{ cm}$$

and the average separation from electrical neutrality over a distance of the order of

the mean free path of the electron is

$$\frac{n_i - n_e}{n} = 1{\cdot}3 \times 10^{-8} \frac{n}{T^3}.$$

This quantity is very small for all reasonable orders of density and temperature which are of interest to us, so that we are justified in assuming that the electron diffusion to the region ahead of the shock front is negligible.

The effect of the radiation from the post-shock gas upon the pre-shock state is determined by its intensity and by the opacity of the gas at the corresponding wavelength. The cosmic medium is composed predominately of hydrogen at a temperature of about 100 K. It thus absorbs radiation of frequency $\nu > \nu_0$, the Lyman limit frequency, and is practically transparent to radiation of frequency $\nu < \nu_0$. The radiation emitted by a gas at a temperature T has a typical frequency of the order of $\nu \sim kT/h$. Thus, at the Lyman limit frequency, the temperature is roughly given by $T \sim 1{\cdot}57 \times 10^5$ K. At temperatures above this critical value, more of the emitted radiation has a frequency $\nu > \nu_0$. However, the opacity of atomic hydrogen in quantum state n is (Allen 1963)

$$\alpha_\nu = \frac{64\pi^4}{3(3)^{1/2}} \frac{me^{10}}{ch^6n^5} \frac{1}{\nu^3} g = 2{\cdot}815 \times 10^{29} \frac{g}{n^5\nu^3}$$

where g is the Gaunt factor of order unity. For the atomic hydrogen in the ground state, the value of α_ν at the Lyman limit is

$$\alpha_{\nu_0} = 6{\cdot}0 \times 10^{-18} \text{ cm}^2 \qquad (g = 0{\cdot}8)$$

and the corresponding photon mean free path, $\lambda_p = 1/n_H\alpha_{\nu_0} = 2{\cdot}4 \times 10^{18}$ cm ($n_H = 0{\cdot}7$). We assumed for simplicity that no appreciable radiation of frequency $\nu > \nu_0$ escapes from the hot region, while for $\nu < \nu_0$ the cool gas is virtually transparent. Thus, a better treatment of ultraviolet radiation is needed for temperatures above those given by the Lyman limit frequency.

References

Allen C W 1963 *Astrophysical Quantities* (London: Athlone) p 99
Courant R and Friedricks K 1948 *Supersonic Flow and Shock Waves* (New York: Wiley) pp 40–4
Field G B 1962 *Interstellar Matter in Galaxies* ed L Wolfier (New York: Benjamin) pp 183–9
Hoskin N E 1964 *Methods in Computational Physics* (New York: Academic Press) pp 265–93
House L 1964 *Astrophys. J. Suppl.* **8** 307–17
Oort J H 1966 *Bull. Astr. Insts Neth.* **18** 421–38
Pottasch S R 1965 *Bull. Astr. Insts Neth.* **18** 7–10
Savedoff M P, Hovenier J W and Van Leer B 1967 *Bull. Astr. Insts Neth.* **19** 107–12
Spitzer L Jr 1962 *Physics of Fully Ionized Gases* (New York: Interscience) p 128
Von Neumann J and Richtmyer R D 1950 *J. appl. Phys.* **21** 232–7